Modelling and Validation of Finite Element Structural Analysis of ISTSat-1

Leonard de Barros Pacheco Seara de Sá

leonard.seara.sa@tecnico.ulisboa.pt

Instituto Superior Técnico, Lisbon, Portugal

December 2021

Abstract

A student developed CubeSat, meant to demonstrate a compact Automatic Dependent Surveillance - Broadcast receiver and antenna, is presented. A Finite Element model of the CubeSat is shown, including all simplifications, elements and boundary conditions. Modal analyses are run, providing the CubeSat's modes, both for correlation purposes and to demonstrate that the fundamental frequency meets the launch authority requirements. The procedures and set-up of an impact hammer modal test campaign are explained, the experimental data is presented, and its good quality is shown. The natural frequencies, damping coefficients and mode shapes are extracted from the experimental data with the use of a modal fitting algorithm. Finally, the experimental modes are correlated to the computational modes with the Modal Assurance Criterion in the [0-1400] Hz range. It is concluded that, despite some issues and discrepancies, the Finite Element Model shows good correlation up to 1000 Hz.

Keywords: CubeSat, Structural Analysis, Finite Element Method, Modal Testing, Validation

1. Introduction

During the launch, all satellites are submitted to extreme mechanical loading conditions and it is necessary to guarantee that all subsystems can endure these loads, and do not break and put the mission at risk of failure. Strict verification tests are performed before any launch, submitting the satellite to similar or even more aggressive conditions than what will be experienced. By having such a conservative approach, one can have confidence that the satellite will endure the launch and safely reach space. However, this may lead to overtesting, resulting in damage, wasted resources and loss of time.

Alternatively, the Finite Elements Method (FEM) might be used to computationally perform structural analysis. FEM is a numerical methodology used to solve differential equations in a continuum by discretizing a domain into a finite collection of subdomains, called 'finite elements' (FE). It has many advantages: result estimates can be obtained before any physical model is built and money is spent; variables can be easily and quickly changed; and the obtained data is not spatially restricted by the placement of sensors. However, FEM programs are just code that take the input provided by the designer, apply all the model equations and mathematical methods to it and return an output. These cannot verify if the approximations done dur-

ing modelling were adequate and whether the model represents faithfully reality.

As such, it is important to validate the FE model, to confirm all assumptions and decisions made. This validation is done by performing some experimental tests, correlating the experimental and computational results, and updating the FE model to better reflect the real system. This raises confidence in all model's results, including results not obtained experimentally. It also allows the implementation of less strict verification tests before launch, reducing costs and the risk of overtesting the satellite. In Figure 1 a diagram representing the sequence followed during a correlation process can be seen. As most correlation criteria require both sets being correlated to have the same size and since the FE model tends to have a greater number of Degrees of Freedom (DoFs), it becomes necessary to reduce the FEA model. If the objective is only to quantify the correlation, the procedure stops at 'Correlation criteria'. Otherwise, the 'FE model update' loop is performed as many times as necessary until a satisfactory level of correlation is attained.

The most common correlation criterion is the Modal Assurance Criterion (MAC) [1].

To obtain good results with correlation criteria, care has to be taken in all steps of the methodology, both on the FE and test segments. To extract
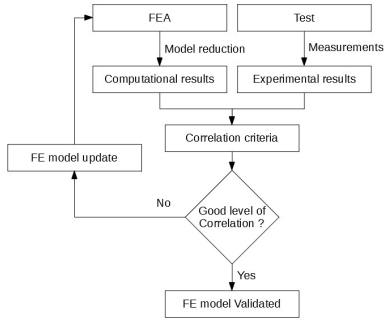
Figure 1: Correlation procedure diagram.

good quality measurements from an experimental test five criteria (sensor location, excitation type, measurement locations, sensor section and excitation location) are considered important [2].

While FE validation has been done on various space missions, such as ESA's BepiColombo spacecraft [3], it is not limited to the space industry, having also been applied in other sectors, such as wind turbines [4].

1.1. CubeSats

CubeSats are nanosatellites (satellites between 1 and 10 kg) that adhere to a standard size and form factor defined by the CubeSat Design Specification (CDS), developed by California Polytechnic State University and Stanford in 1999 [5]. The unit size of a CubeSat is a 10cm side cube, called 1U, with a mass of up to 2kg.

This standard was created to simplify development, provide safe deployment and operation, reduce costs and make space more accessible. This standardization also makes possible the mass production of components and for companies to offer off-the-shelf components which can easily be integrated on the CubeSats. By being cheaper, one can have a larger number of satellites, allowing for an easier set-up of a constellation. Their small size also allow CubeSats to more easily hitch rides as secondary loads on rockets transporting other cargo. On the other hand, the reduced available space for systems puts a limit on the complexity and number of subsystems on board and by being mostly secondary cargo, the launch of CubeSats is highly dependent on other missions' schedules.

During the launch, the CubeSats are transported inside a deployer attached to the launch vehicle, which releases it into space when appropriate.

This type of satellite has become quite popular among university teams. And like any other satellite, structural data is needed to guarantee structural integrity and mission success. Some universities, with projects still in an initial phase, use only FEA [6]. Despite costs, time constraints and absence of access to testing facilities that limit test-

ing in many teams, others have performed vibration tests with their CubeSats, although the data was not used to improve and validate FE models [7]. Finally, while not as common, some teams have correlated experimental and computational results through the use of correlation criteria and validated their FE model [8].

1.2. ISTSat

ISTSat is a team of students, professors, researchers and radio amateurs based at Instituto Superior Técnico (IST), University of Lisbon, that develops CubeSats. ISTSat-1 is the first CubeSat developed by the ISTSat team, and also the first university CubeSat project developed in Portugal. It is a 1U CubeSat and most ISTSat-1 subsystems have been designed and built in-house. ISTSat-1 is meant to demonstrate a compact Automatic Dependent Surveillance - Broadcast (ADS-B) receiver and antenna, used to track the position and status broadcast by commercial aircraft [9].

2. Theoretical Background

2.1. Equation of Motion

The equation of motion of any dynamic system is given by

$$[M]\{\ddot{x}(t)\} + [C]\{\dot{x}(t)\} + [K]\{x(t)\} = \{f(t)\}\,, \quad (1)$$

where $[M]$, $[C]$ and $[K]$ are the mass, damping and stiffness matrices, respectively; and $\{x(t)\}$ and $\{f(t)\}$ are the generalized coordinates and force column vectors, respectively [10].

The natural frequencies of a system are the frequencies at which the system will naturally oscillate if subjected to a disturbance and no damping or external forces exist. Each natural frequency has a mode shape associated, i.e., the system motion that happens when it vibrates at that frequency. The natural frequencies, damping coefficients and mode shapes are called modal parameters and are a function of the structural and material properties and the boundary conditions.

To obtain the natural frequencies of the structure, the undamped free vibration of the system is analysed

$$[M]\{\ddot{x}\} + [K]\{x\} = \{0\}\,. \quad (2)$$

When a solution of the form $x = X\sin(\omega t)$, where X is the amplitude and ω the angular frequency, is considered, the solution yields the natural frequencies and mode shapes of the system. There are as many natural frequencies as there are DoFs and the first one is called fundamental frequency. If one of the frequencies is zero, then there is a rigid-body mode.

When $[M]$ and $[K]$ are transformed into modal coordinates the Rayleigh's equation is obtained

$$\omega_j^2 = \frac{[\Phi_i]^T[K][\Phi_j]}{[\Phi_i]^T[M][\Phi_j]}, \qquad (3)$$

that shows that when the system becomes overall stiffer, the natural frequencies will rise, and will become lower if the system gains more mass.

Not all modes are equally important. Some modes are more easily excited and others might only be excited if the excitation forced is applied in a certain direction. To better evaluate the importance of a specific mode in the overall response, instead of modal mass, the effective modal mass, m_{eff}, is used [11]. Whenever a excitation is applied to the structure, the modes with higher m_{eff} will be more easily excited and will have bigger impact on the overall response. Usually, the first modes tend to have bigger effective mass and bigger influence. For each direction there is an associated m_{eff}, in a total of six per mode, 3 in translation (axis X, Y and Z) and 3 in rotation (around axis X, Y, Z).

2.2. Response in Time and Frequency Domains

When using exciters, accelerometers or other sensors, the input and response are measured in the time domain. But to be able to directly assess which are the main frequencies of the signal, one might wish to study the signal in the frequency domain.

The Fourier Transform (FT) allows the transformation of a function from the time to the frequency domain [12]. However, when measuring results, the data is not measured continuously, but at discrete points in time. So the Discrete Fourier Transform (DFT) is used instead. Being a discrete and finite sequence of values, it can be easily implement and done by computer algorithms, named Fast Fourier Transform (FFT) algorithms.

After applying the FFT to the measured data, linear spectra of both the input excitation and output response are obtained. From these, the input, S_{XX}, and output power spectra, S_{YY}, can be computed, representing the power distribution of the input and output over the spectrum; and also the cross-spectrum, S_{XY}, representing the cross-correlation between signals. From these the Frequency Response Function (FRF), a complex function, typically represented as H, is obtained and represents the ratio between the input excitation force and output response motion of a system in the frequency domain.

When represented in terms of amplitude and phase, in the amplitude plot, the peaks are found at the resonance frequencies, while in the phase diagram, at resonance the phase loses 180° and at anti-resonances the phase gains 180° instead.

The coherence function is a function in frequency used to assess the quality of the measured data and is given by

$$\gamma_{XY}^2(f) = \frac{|S_{XY}(f)|^2}{S_{XX}(f) \cdot S_{YY}(f)}. \qquad (4)$$

It correlates the input spectrum to the output spectrum and defines how much the second is due to the first, indicating how repeatable the measurement of the FRF is. Each time a measurement is done, the new power spectra are computed and are averaged with the previous spectra, and new values of coherence are obtained. It can vary between 0 and 1, where 1 indicates that the FRF measurements are very repeatable, and 0 indicating the opposite. Ideally, it is desirable for the coherence to be 1 for the entire measured frequency range. At anti-resonance frequencies, the output data tends to be so low that the noise of the instruments becomes of the same order of the output and inconsistency between measurements is expected, and values closer to zero are not problematic.

2.3. Modal Assurance Criterion

The MAC gives a scalar value indicating the amount of correlation between two vectors and is defined as

$$\text{MAC} = \frac{|\Phi_i^H \Phi_j|^2}{(\Phi_i^H \Phi_i)(\Phi_j^H \Phi_j)}, \qquad (5)$$

where Φ_i and Φ_j are the two modal vectors being correlated.

The MAC varies between 0 and 1, with 1 indicating an high degree of consistency. The MAC is not an orthogonality check, as the modal vectors are orthogonal in respect to the mass and stiffness matrices, which are not used in the MAC expression.

For space applications and as suggested by the ECSS Standard [13], there is good correlation between the computational model and the test model if for the fundamental modes the MAC is greater than 0.9 (and frequency difference lower than 3%); for modes with $m_{\text{eff}} > 10\%$ the MAC is greater than 0.85 (and frequency difference lower than 5%); and MAC greater than 0.8 (and frequency difference lower than 10%) for the remaining modes in the relevant frequency range.

3. Modelling and FE Analysis

In figure 2, an exploded view of the ISTSat-1 is presented and all subsystems are identified. The same cartesian positive coordinate system is always used for the system as a whole and is defined as follows: with the origin in the centre of the CubeSat, the +Z axis is normal to the V/UHF Antenna and the +X axis points to the side frame with the Remove Before Flight (RBF) pin gap.
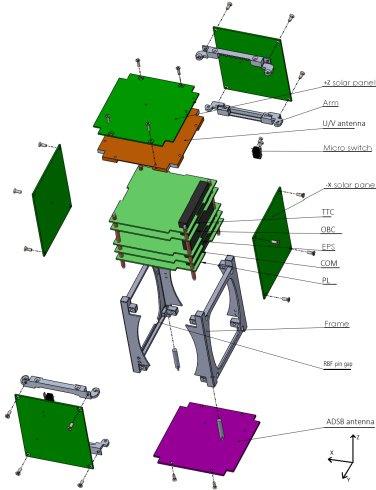
Figure 2: ISTSat-1 exploded view.

The main body structure, composed of four arm links and two side frames, is made of aluminium 7075-T6. The side frames are mostly symmetrical and contain the rails and rail stand-offs that are in contact with the dispenser. On the +X side frame, there is also a small opening for the RBF pin. The arm links connect the side frames, making the assemblage of all other subsystems possible. The four axes, made of stainless steel, are located on each corner of the PCBs and support the entire PCB stack.

On the PCB stack there are a total of five PCBs, all with approximately the same size and shape (about 95 x 90 x 1.6 mm). These boards are made of composite FR4 and copper. PC/104 connectors on each PCB connect them all electrically. Starting from the top PCB (+Z), there is the TTC (Telemetry, Tracking and Communications), the OBC (On-Board Computer), the EPS (Energy Power System), the COM (Communication Processor and Data Storage) subsystem and the PL (Payload), corresponding to the ADS-B receiver. Attached to the EPS PCB is a battery pack, composed of four Lithium-Ion polymer cells.

On all faces of the satellite, with exception of the -Z face, solar panels (SP) are fastened to the structure. Each SP substrate corresponds to a normal PCB, where the cells are attached. On the +Z face, beneath the SP a Very/Ultra High Frequency (V/UHF) antenna is mounted. On the -Z face is located the ADS-B antenna, made of Rogers RT/duroid 6010, a ceramic-PTFE laminate composite.

3.1. CAD modelling and idealization

The initial CAD model of the ISTSat-1 was created in *SOLIDWORKS*, where all subsystems were modelled in full detail. This model was then ported

to SIEMENS NX, where a process of idealization was conducted, simplifying the model. The process of idealization is a process of compromises and equilibrium between having a model that represents faithfully reality and the computational and time constraints imposed by a greater level of detail.

Almost all side frame and link arms' fillets were removed. All bolt holes were left in the idealized model, but the chamfers that were modelled to allow space for the bolt heads were removed.

The PCB subsystems, besides the board itself, have integrated multiple electronic components. Since these components have incredibly small dimensions and for the system response the most relevant factor is the overall mass and stiffness of the PCB system, only the board itself of each PCB component was modelled, albeit including the non-modelled components' mass. The exceptions are the PC/104 connectors (made of Polyphenylene sulfide - PPS), as they have a more significant dimension and add additional constraints and stiffness to the PCB Stack; and the Battery Pack since in the system PCB + battery, the battery has 72% of the mass.

Since during experimental tests the SPs were replaced by same sized PCBs without cells, as these components are quite fragile, the solar cells were also removed in the idealized model.

The PCBs, the SPs and the ADS-B antenna are characterized by the difference in order of magnitude between the height and the remaining two dimensions and can, therefore, be considered bi dimensional (the results are constant throughout the height, with changes only along the width and length). This reduced part of the model from 3D to 2D, with associated computational resources gains.

For the VHF/UHF antenna, only the antenna structure was considered.
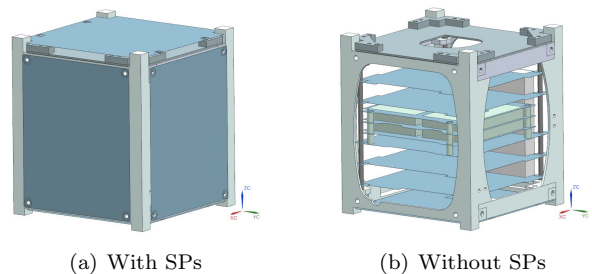
The final idealized model can be seen in figure 3.

(a) With SPs   (b) Without SPs

Figure 3: Idealized model.

3.2. FEM modelling

Once the idealization process was complete, the FE model was created in SIEMENS NX.

The materials that were used in the simulation are presented in Table 1. In this work, all materials

4

were considered to be linear. For the PCBs, different densities were assigned, so that each PCB has the total weight of the respective subsystem. A battery is a complex component with various materials, but since structurally the most relevant material is the casing material, the batteries were considered to be made only of polyethylene (PE). The ADS-B antenna is considered to be uniform across the area and is made of Rogers RT/duroid 6010. However, since during the tests the patch antenna was substituted by a PCB similar to that of a solar panel, the material assigned to the antenna was the same as for the SP. All modelled bolts are made of stainless steel.

As previously mentioned, the basis of the FEM is the division of the model into smaller segments called elements, with a group of elements being called a mesh. All data regarding elements was taken from [14]. For the solid bodies (e.g., the side frames) CTETRA and CHEXA elements were used. Since the PCBs and other components are considered bi-dimensional, 2D elements, namely CTRIA3 and CQUAD4, were used.

For the bolts, CBAR elements were used for the shank and RBE2 elements connected the CBAR elements to the other components. An exterior concentrated mass point, which is a 0D element, was added to the model and connected by RBE2 elements to the -Z faces of the side frames standoffs and the CubeSat's side frames edges, only for the hard mounted configuration analyses. Finally, additional concentrated mass points were added, emulating the accelerometers masses (2.4 and 4.8 grams) attached during the modal tests. The positions of these elements corresponded to the accelerometers' positions, specified in section 4.

A simple linear static analysis was run to verify convergence of the results, as usually, these are the most simple and fastest analyses to run. It was also used to verify that the entire model had been correctly set up and that a non linear analysis was not necessary.

3.3. Loads and Boundary Conditions
A pre-load of 2000 N was applied to all bolts. In modal analysis, no external loads are applied.

As for the boundary conditions, these depended on the type of analysis that was intended. As mentioned previously, the CubeSat will be transported inside a deployer. However, to simplify the FE model, in the FEA simulating launch conditions, the dispenser will be neglected and not modelled. This can be seen as the CubeSat being attached directly to the launch vehicle. On the analysis simulating the launch, rigid elements connected the side frames edges and stand-off bases to an external node. These four edges and four faces were chosen

as they will be the CubeSat parts that will be in contact with the dispenser during launch and to avoid over constraining the model. This way the side frames are still able to deform and both the PCBs and solar panels have no constraints besides the connections to other components. This configuration is known as 'hard-mounted configuration'. The external node was fixed in all six DoF. For the correlation purposed analysis, free-free conditions were used instead and no DoFs had additional restrictions.

Table 1: Material mechanical properties.

	ρ (kg/m^3)	E (GPa)	ν	G (GPa)	σ_{yield} (MPa)
Aluminium 7075-T6	2810	72	0.33	26.9	503
FR4	6093 (TTC) 3913 (OBC) 5401 (EPS) 4174 (COM) 3431 (PL) 1840 (SP) 1883 (Battery)	24 (x) 21 (y) 21 (z)	0.12 (xy) 0.12 (xz) 0.13 (yz)	10.71 (xy) 10.71 (xz) 9.29 (yz)	276
PPS	1550	11.5	0.3	4.4	70
PE	1883.69	1	0.4	0.36	28
Stainless Steel	7872	200	0.25	76.92	490

3.4. Results - Hard mounted configuration
The modes that are derived from this analysis serve as the foundation for all dynamic analyses, such as response in frequency and random vibration.

During the launch, the loads induced by the launcher will have frequencies concentrated on the range [20,2000] Hz. For this range, there were a total of 77 modes, with 52 of these having more than 0.1% of modal effective mass fraction.

In Table 2 the initial modes are presented. The frequency, the modal effective mass fraction in the three translation axis and a brief description of the mode are given.

Table 2: ISTsat-1 initial modes in hard-mounted configuration.

Mode	Freq (Hz)	Effective modal mass fraction			Mode description
		X	Y	Z	
1	346.4	8.9E-08	3.4E-06	0.096	TTC
2	413.8	0.0018	0.0010	0.17	COM
3	428.5	2.8E-05	0.0038	0.076	OBC & COM
4	437.7	0.0070	0.026	0.057	OBC & EPS
5	485.9	6.4E-04	0.31	0.025	PL & EPS
6	493.1	0.0013	0.074	0.0049	PL
8	498.5	0.049	6.1E-06	3.7E-05	±X SP
9	503.7	0.0012	3.9E-04	7.5E-04	±Y SP
11	572.2	0.15	0.010	0.027	ADS-B Ant.
14	586.6	6.4E-04	2.5E-06	0.029	+Z SP

5

Table 3: FEA PL modes in free-free condition.

Mode	Frequency (Hz)
1	407.9
2	631.2
3	748.2
4	762.3
5	1168.8
6	1195.4
7	1206.3
8	1280.8
9	1352.5

Table 4: FEA EPS modes in free-free condition.

Mode	Frequency (Hz)
1	483.2
2	515.3
3	607.9
4	703.0
5	753.8
6	875.6
7	1008.8
8	1069.7

The first modes are all related to the PCBs Boards. The TTC is the board with the lowest frequency, 346.44 Hz, also known as the fundamental frequency. This frequency is above the level required by the launch authority.

It was also seen that, in all directions, the higher the frequency of the mode the smaller the $\hat{m}_{eff_j}$ became, proving that the initial modes are more relevant.

3.5. Results - Free-free condition

For the free-free condition analyses, due to experimental limitations, the computed frequency range went from 0 to 1300 Hz.

As further explained in section 4, each component set-up and measurement was made sequentially and individually. This means that multiple simulations were run and that the addition of mass corresponding to the accelerometers was made separately across simulations (e.g., in the PL-focused analysis the masses were only added to the PL).

In Tables 3, 4 and 5, are presented all the modes frequencies for the free-free conditions analyses of the PL, EPS and +Y components, respectively.

For simplicity of notation, and since each component was analysed separately, the numbering for the modes of each component will be done independently. For example, the PL mode 1 is not the first global mode of the system, but the first PL mode that was obtained on the simulation where the accelerometers' mass was added to the PL.

Table 5: FEA +Y SP modes in free-free condition.

Mode	Frequency (Hz)
1	347.3
2	636.8
3	693.5
4	710.1
5	843.3
6	1352.8

Looking at the first mode frequency of each component and comparing it with Table 2, it can be seen that all these frequencies had a downwards shift when compared with the respective component and frequency. Since additional mass was added in these free-free simulations, from equation 3, one can see that this shift is expected and serves as a further check that the mass addition was defined correctly.

4. Modal Test

Modal tests with the ISTSat-1 were conducted to obtain the CubeSat's experimental modal parameters.

4.1. System Under Test

The system under test was a non-functional replica of the ISTSat-1, including the entirety of the structure, the PCB Stack and all fasteners connecting the aforementioned components. The differences to the CubeSat to be launched were as follow: the SPs were replaced by dummy SPs, without photovoltaic cells; the ADS-B antenna was replaced by a dummy ADS-B antenna, made of FR4 instead of ceramic subtract; and all wiring connecting the various subsystems, the ADS-B antenna and the SPs were not installed.

The dummy components were dimensionally equal to the real subsystems and had similar properties, only being substituted for precaution.

4.2. Test Set Up
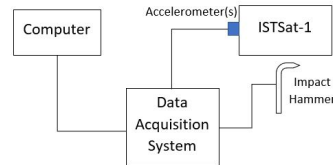
The test set-up schematic can be seen in Figure 4.

Figure 4: Test set-up schematic.

To emulate free-free conditions, the CubeSat was suspended from above with fishing line, an elastic material that allows the CubeSat to vibrate as freely as possible when excited.

An impact hammer was used to excite the CubeSat. A plastic tip was used, with a nominal frequency range from 0 to 2000 Hz. The used accelerometers were unidimensional and the measurement direction was always normal to the surface where they were attached. The computer software used for visualization and processing of the measured data was Brüel & Kjær - Pulse LabShop Version 22.2.0.98.

For each measurement position, the CubeSat was hit five times, with the resulting FRFs being averages of the response on the five hits, allowing for

the computation of the coherence function. An exponential window with a shift of 500 μs and a τ of 10 ms was applied to all accelerometer measurements and a transient window with a shift of 1 ms and a length of 3 ms was applied to the impact hammer measurement.

Considering the relative independence between components seen in the FEM, the various components results were analysed independently. The +Y SP was the only SP that was tested. For the PCB stack, only the PL and EPS PCBs were tested. The other PCBs were not measured because both the distance between each PCB and the accelerometers height were 10 mm, which meant there was not enough space between PCBs. Removing one of the boards to allow for more space was not feasible as it would change the overall stiffness of the entire stack. To be possible to excite the PCBs with the impact hammer, the ADS-B antenna was removed. In the EPS, due to the battery pack, there was a single small space near the axes (-X,-Y) where an accelerometer could be attached. The positions of the accelerometers can be seen in Figure 5.
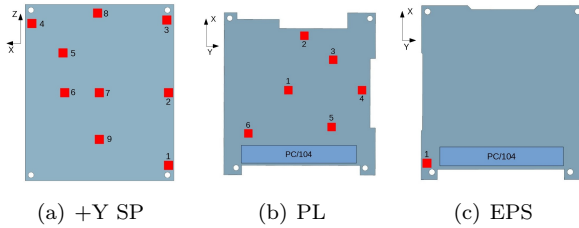

(a) +Y SP   (b) PL   (c) EPS

Figure 5: Accelerometers positions.

4.3. Experimental Results

The coherence of all accelerometers on the three measured components are shown in Figures 6, 7 and 8.
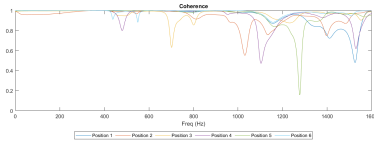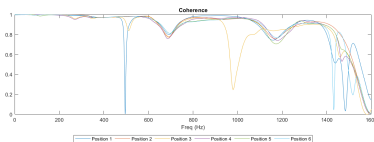

Figure 6: Coherence: PL.

Figure 7: Coherence: +Y SP.

For the PL and +Y SP, it can be seen that the coherence functions are close to one across most of
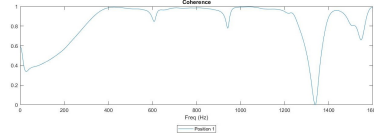

Figure 8: Coherence: EPS position 1.

the spectrum up to 1000 Hz for all positions. While there are some dips in coherence before 1000 Hz, these become more frequent and general degradation of the coherence occurs above this frequency. This can be seen as evidence that the tip that was used for excitation, did not excite the frequencies above 1000 Hz as well as those below. As such, lower quality modal fitting is expected for frequencies above 1000 Hz.

For the EPS, while coherence was low up to 400 Hz, as the first peak in the response was only encountered above this frequency, this reduced coherence is not of much concern. For the remaining spectrum, the coherence stays close to one, except for three frequencies where antiresonance occurs, including a significant dip around 1300 Hz.

For every accelerometer position, a different FRF was obtained.

4.4. Modal fitting

With the FRFs for each component, the modal parameters were extracted for each component individually through the application of the LSRF method [15], which is implemented in MATLAB. For this algorithm it is necessary to provide the measured FRFs, the corresponding frequencies, the sample rate and an estimate of the number of modes to be found. The output of this algorithm, corresponds to the natural frequencies, the damping coefficients for each mode, the mode shape vectors and the reconstructed FRFs based on the previous outputs.

The success of the modal fitting is assessed through comparison of the reconstructed and experimental FRFs. If either too many or too few modes are estimated the FRFs will not match.

For the PL, ten modes were extracted from the [100,1400] Hz range; for the +Y SP, seven modes from [100,1300] Hz; and for the EPS, eight modes from [100,1200] Hz. These ranges were chosen as they provided the best fitting. The frequencies and mode damping coefficients for each component can be seen in Tables 6, 7 and 8.

For the PL and EPS, all modes have a damping coefficient of around 0.05 (5%), which is a typical value, while in the +Y SP there are a couple of modes with higher than usual damping.

The experimental and reconstructed FRFs for PL position 1 can be seen in Figure 9, which show a relatively good fit on both the magnitude and

Table 6: PL extracted modes.

Mode	Freq Hz	Mode damping
1	365.8	0.072
2	517.6	0.046
3	651.8	0.071
4	686.5	0.050
5	831.6	0.044
6	948.6	0.052
7	1062.2	0.032
8	1155.0	0.033
9	1258.7	0.027
10	1356.0	0.023

Table 7: +Y SP extracted modes.

Mode	Freq Hz	Mode damping
1	361.3	0.086
2	503.5	0.174
3	641.7	0.229
4	730.7	0.051
5	921.6	0.035
6	1071.9	0.035
7	1152.8	0.050

Table 8: EPS extracted modes.

Mode	Frequency (Hz)	Mode damping
1	452.2	0.044
2	550.3	0.082
3	624.8	0.028
4	694.5	0.036
5	764.2	0.023
6	971.9	0.028
7	1055.1	0.028
8	1091.7	0.033

phase, with no missing peaks in the reconstructed FRF. For the other accelerometers, the same quality matches were obtained.
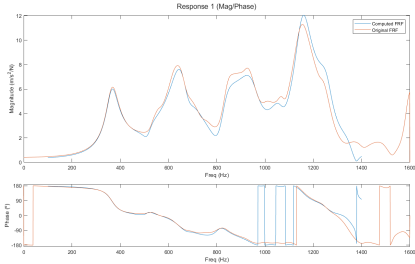

Figure 9: Experimental and reconstructed FRFs: PL position 1.

For +Y SP accelerometers, it was verified that while the match between measured and reconstructed FRFs did not have the same quality as it was obtained for the PL subsystem, all modes were still extracted, with no missing relevant peak.

For the EPS, the match was almost perfect, as there was only one FRF to curve fit to. Nevertheless, this almost-perfect match does not guarantee that all modes of the EPS were extracted, as modes where the measured point corresponds to a nodal point do not appear and therefore cannot be extracted.

5. FE-Experimental Correlation

With both the computational and the experimental results it becomes possible to compare both sets of results and validate the FE model.

To be able to use the MAC, both mode shapes need to be the same size. Since the FE model has hundreds of thousands of DoFs more than the experimental results FE model, it has to be reduced. Since the used correlation metric is the MAC, which does not take into account the mass matrix, it is only necessary to compute the mode shapes and choose the DoFs that are located at the accelerometers' positions, with no further manipulation.

5.1. Frequency Comparison and MAC

The difference between the computational (f_{FE}) and experimental (f_{EXP}) mode frequencies, in percentage, is given by

$$\mathrm{dif} = \frac{f_{\mathrm{FE}} - f_{\mathrm{EXP}}}{f_{\mathrm{FE}}} \times 100 \qquad (6)$$

For the PL, when comparing the 10 experimental modes in Table 6 to the 9 FEA modes in Table 3, the MAC matrix in Figure 10 is obtained. The three first modes of each set seem to be strongly correlated with diagonal terms close to 1 and off-diagonal terms close to zero. For the upper modes, the correlation between modes becomes less clear.

Figure 10: MAC of all PL modes.

Some experimental modes, like modes 5 or 7, do not have a good enough correlation to any FEA mode, which can indicate that these modes were not correctly estimated by the modal fitting algorithm.

Other FEA modes, like modes 8 or 9, have higher MAC for various experimental modes. From the shapes of mode 8 and 9 (figures 11 and 12), it can be seen that in the PL, both modes have very similar shapes, and what distinguishes them are the shapes at the other components. So it is not possible to accurately correlate higher frequency modes while only measuring one PCB.

In the end, there are 6 modes that can be more clearly correlated. The new MAC matrix with only these 6 modes can be seen in Figure 13. Most of the off-diagonal terms are close to zero, while in the diagonal, with exception of FEA mode 7, all modes are above 0.8. The frequency difference can be seen in Table 9.
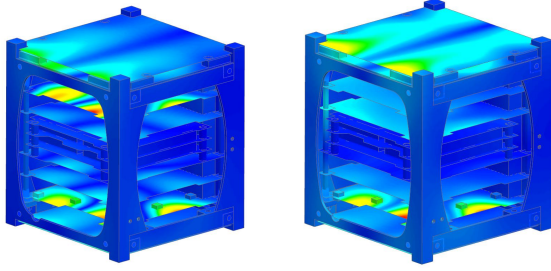
8

Figure 11: FE PL mode 8.

Figure 12: FE PL mode 9.

FEM	1	2	3	7	8	6
EXP Frequency	407.9	631.2	748.2	1206.3	1280.8	1168.8
1	365.84	0.954	0.042	0.005	0.009	0.017	0.027
2	517.61	0.004	0.898	0.079	0.010	0.007	0.009
3	651.81	0.010	0.042	0.915	0.092	0.021	0.015
6	948.62	0.049	0.057	0.201	0.617	0.062	0.061
9	1258.7	0.052	0.006	0.009	0.023	0.814	0.563
10	1356	0.047	0.096	0.017	0.183	0.585	0.810

Figure 13: MAC of selected PL modes.

Table 9: +Y SP mode frequencies comparison.

FEA Mode	FEA freq Hz	Experimental Mode	Experimental freq Hz	Difference between freqs (%)
1	407.9	1	365.8	10.31
3	631.2	2	517.6	18.00
4	748.2	3	651.8	12.88
7	1206.3	6	948.6	21.36
8	1280.8	9	1258.7	1.73
6	1168.8	10	1356.0	-16.02

With exception of FEA mode 7, all correlated modes have frequency differences less than 20%. In most cases, except for FEA mode 6, the FEA modes had higher frequencies.

For the +Y SP, when comparing the 7 experimental modes in Table 7 to the 6 FEA modes in Table 5, the MAC matrix in Figure 14 is obtained.

FEM	1	2	3	4	5	6
EXP Frequency	347.3	636.8	693.5	710.1	843.3	1352.8
1	361.3	0.913	0.024	0.054	0.065	0.029	0.010
2	503.5	0.295	0.081	0.605	0.657	0.025	0.137
3	641.7	0.338	0.119	0.532	0.579	0.061	0.103
4	730.7	0.043	0.777	0.051	0.139	0.163	0.020
5	921.6	0.345	0.170	0.389	0.406	0.017	0.021
6	1071.9	0.194	0.207	0.417	0.325	0.022	0.010
7	1152.8	0.137	0.298	0.201	0.218	0.175	0.040

Figure 14: MAC of all +Y SP modes.

For the +Y SP, the correlations levels were not as good as they were for the PL. While the correlation is clear for the first modes of both the FEA and experimental results, for the higher frequency modes (FEA modes 5 and 6, experimental modes 5, 6 and 7) there was no correlation at all. For the intermediate frequencies, there was some level of correlation.

Looking at just the modes with correlation and reordering them, the new MAC matrix with only 4 modes can be seen in Figure 15. FEA modes 3 and 4 have similar MAC values for diagonal and non-diagonal MAC values, indicating the possible need for a greater number of accelerometers so that they can be clearly distinguished.

FEM	1	3	4	2
EXP Frequency	347.3	693.5	710.1	636.8
1	361.3	0.913	0.054	0.065	0.024
2	503.5	0.295	0.605	0.657	0.081
3	641.7	0.338	0.532	0.579	0.119
4	730.7	0.043	0.051	0.139	0.777

Figure 15: MAC of selected +Y SP modes.

The frequency difference between the correlated modes can be seen in Table 10.

Table 10: +Y SP mode frequencies comparison.

FEA Mode	FEA freq Hz	Experimental Mode	Experimental freq Hz	Difference between freqs (%)
1	347.3	1	361.3	3.87
3	693.5	2	503.5	-37.74
4	710.1	3	641.7	-10.66
2	636.8	4	730.7	12.85

With exception of the first mode, all correlated modes have significant frequency shifts, above 10%, showing less good quality results for the +Y SP.

For the EPS, the comparison between the FEA and experimental modes is shown in Table 11. As no mode shapes were available to apply the MAC to, only the frequencies were compared.

Table 11: EPS mode frequencies comparison.

FEA Mode	FEA freq Hz	Experimental Mode	Experimental freq Hz	Difference between freqs (%)
1	483.2	1	452.2	6.42
2	515.3	2	550.3	-6.79
3	607.9	3	624.8	-2.78
4	703.0	4	694.5	1.21
5	753.8	5	764.2	-1.38
6	875.6	6	971.9	-11.0
7	1008.8	7	1055.1	-4.59
8	1069.7	8	1091.7	-2.05

Assuming that all experimental modes had correspondence to the FEA modes in the same order, all modes, except for one, had frequency differences less than 10%.

5.2. Discussion

Comparing the MAC and the frequency shifts with the levels indicated in the ECSS Standard [13], for PL mode 1 the MAC was greater than 0.9 but the frequency shift was also greater than 3%. For the remaining modes, with exception of FEA mode 7, all met the requirement of MAC greater than 0.8; for the frequency deviation, which was to be below 10%, all failed, except for FEA mode 8. As such, good correlation was verified for most modes, especially those below 1000 Hz. While the MAC level fulfilled the ECSS requirements, proving mode shape similarity, the frequency shifts were more significant and did not meet the standard requirements overall, indicating the need to adjust the material stiffness in the FEA. Since for most modes the FEA frequency was higher, it can be concluded that the PL is over stiff in the FE model and the stiffness has to be reduced.

For the +Y SP mode 1, the MAC was greater than 0.9 and it almost met the frequency shift requirement of 3%, showing good correlation. For the remaining modes, neither the MAC levels nor the frequency shifts met the proposed levels. This shows that there is a poorer correlation between the +Y SP FEA and experimental modes, indicating flaws either in the FEA model or in the experimental data measurements, not allowing to have full confidence in the FEA results as they currently are, requiring further study and testing. This lower correlation quality might result from: issues with the FE model, possibly in the way the connection between the solar panels and the structure was modelled or in the assumption of the solar panels as uniform boards; the way the CubeSat was suspended during +Y SP testing, that induced a lateral oscillation of the CubeSat of some magnitude, making it harder to hit consistently.

As for the EPS, despite having lower frequency shifts, the lack of MAC did not allow to take more meaningful conclusions about mode correlation. However, for most modes, it can be seen that FEA frequency was lower than the experimental one, meaning that in the FEA, the EPS was less stiff than the real one.

6. Conclusions

The results for the modal analysis in hard mounted configuration showed that the CubeSat met the launch authority requirements regarding the fundamental frequency, with enough margin to accommodate any errors in the analysis.

While the hammer excitation and accelerometers impose physical limitations in the modal tests, due to relative size and mass when compared with the CubeSat, it was still possible to obtain good coherence measurements, and FRFs with clear peaks associated to the modes up to 1300 Hz.

When comparing computational and experimental frequencies and mode shapes, although not all ECSS requirements were met, it was still possible to infer correlation between the FE and the experimental models (albeit in need of some FE model updates - see figure 1), increasing confidence in all obtained FE results.

Finally, despite the need for further testing and analysis, it can be concluded that it is feasible, with a promising future potential, the use of impact hammer testing in order to obtain validated CubeSats FEM models at a reduce amount of time and resources, despite the many physical limitations and reduced spacecraft size, increasing the confidence in FEA and reducing the need for an aggressive test campaign that might needlessly overstress the CubeSat before launch.

References

[1] R. J. Allemang. The modal assurance criterion - Twenty years of use and abuse. *Sound & vibration*, 37:14–23, August 2003.

[2] T. G. Carne and C. R. Dohrmann. A modal test design strategy for model correlation. Technical Report SAND-94-2702C; CONF-950240-4, Sandia National Labs., Albuquerque, NM (United States), December 1994.

[3] J. F. Mercer, A. M. Kiley, and G. S. Aglietti. BepiColombo: sine test FEM correlation experiences. In *Proceedings of ISMA2014*, volume Proceedings of ISMA2014 of *Dynamics of aerospace structures*, pages 835–849, Leuven, September 2014.

[4] S. Manzato, B. Peeters, R. Osgood, and M. Luczak. Wind turbine model validation by full-scale vibration test. *European Wind Energy Conference and Exhibition 2010, EWEC 2010*, 5, January 2010.

[5] Cal Poly – San Luis Obispo CA. CubeSat Design Specification Rev 14, July 2020.

[6] B. Kelsey, C. Anderson, N. Petilli, and R. Cuerdon. Mechanical Design, Structural and Thermal Analysis for a 6U eLEO CubeSat. Master's thesis, Worcester Polytechnic Institute, Massachusetts, USA, March 2020.

[7] A. Ampatzoglou and V. Kostopoulos. Design, Analysis, Optimization, Manufacturing, and Testing of a 2U Cubesat. *International Journal of Aerospace Engineering*, June 2018.

[8] G. Pierlot. Oufti-1 : flight system configuration and structural analysis. Master's thesis, University of Liège, Liège, Belgium, June 2009.

[9] J. P. Monteiro, R. Afonso, and J. Pinto. ISTSat-1 – The First Portuguese University CubeSat. *13th Congress of the Portuguese Comitee of URSI*, 2019.

[10] Singiresu S. R. *Mechanical Vibrations*. Prentice Hall, 5th edition, 2011.

[11] T. Irvine. Modal Participation Factor, December 2015.

[12] R. Bracewell. *The Fourier Transform & Its Applications*. McGraw-Hill, 3rd edition, June 1999.

[13] ESA ECSS Secretariat. ECSS-E-ST-32-11C - Modal survey assessment, July 2008.

[14] SIEMENS. Element library reference, 2014.

[15] A. A. Ozdemir and S. Gumussoy. Transfer Function Estimation in System Identification Toolbox via Vector Fitting. *IFAC-PapersOnLine*, 50(1):6232–6237, July 2017.